This is a "preproof" accepted article for *Mineralogical Magazine*.
This version may be subject to change during the production process.
10.1180/mgm.2025.1

Tarutinoite, $Ag_3Pb_7Bi_7S_{19}$, a new member of the lillianite homologous series from the Tarutinskoe copper-skarn deposit, Southern Urals, Russia

Anatoly V. Kasatkin[1]*, Cristian Biagioni[2], Fabrizio Nestola[3], Radek Škoda[4], Vladislav V. Gurzhiy[5], Atali A. Agakhanov[1], and Aleksey M. Kuznetsov[6]

[1]Fersman Mineralogical Museum of the Russian Academy of Sciences, Leninsky Prospekt 18-2, 119071 Moscow, Russia;
[2]Dipartimento di Scienze della Terra, Università di Pisa, Via Santa Maria 53, I-56126 Pisa, Italy;
[3]Dipartimento di Geoscienze, Università di Padova, Via Gradenigo 6, I-35131, Padova, Italy;
[4]Department of Geological Sciences, Faculty of Science, Masaryk University, Kotlářská 2, 611 37, Brno, Czech Republic;
[5]Institute of Earth Sciences, St. Petersburg State University, University Emb. 7/9, 199034 Saint-Petersburg, Russia;
[6]Oktyabrskaya str., 5-337, 454071 Chelyabinsk, Russia

*Author for correspondence: Anatoly V. Kasatkin, E-mail: anatoly.kasatkin@gmail.com
Running title: Tarutinoite, a new member of the lillianite homologous series

Abstract

The new mineral tarutinoite, ideally $Ag_3Pb_7Bi_7S_{19}$, was found in a fragment of a drill core extracted at 178.5 m level of borehole #4604 at the Tarutinskoe (Tarutino) copper-skarn deposit, Chelyabinsk Oblast, Southern Urals, Russia. It occurs as anhedral grains up to 0.10 × 0.05 mm intergrown with hessite and galena in magnetite and calcite. Tarutinoite is grey, opaque with metallic luster, brittle tenacity and uneven fracture. No cleavage and parting are observed. The Vickers' micro-indentation hardness (VHN, 25 g load) is 178 kg/mm^2 (range 165–194, n = 4), corresponding to a Mohs' hardness of 3.5–4, and calculated density is 7.180 g/cm^3. In reflected light, tarutinoite is greyish-white, very weakly bireflectant and non-pleochroic. In crossed

polarizers the new mineral exhibits moderate anisotropy, in grey and dark grey tones with bluish tints. The reflectance values for wavelengths recommended by the Commission on Ore Mineralogy of the International Mineralogical Association are (R_{min}/R_{max}, %): 45.5/47.9 (470 nm), 43.5/45.0 (546 nm), 43.3/44.1 (589 nm) and 41.8/42.5 (650 nm). The chemical composition (wt.%, electron microprobe data, mean of 7 spot analyses) is Cu 0.30, Ag 8.33, Cd 0.04, Pb 37.12, Bi 37.52, S 15.15, Se 0.40, Te 0.66, total 99.52. The empirical formula calculated on the basis of 36 atoms per formula unit is $(Ag_{3.01}Cu_{0.18})_{\Sigma 3.19}(Pb_{6.98}Cd_{0.01})_{\Sigma 6.99}Bi_{7.00}(S_{18.42}Se_{0.20}Te_{0.20})_{\Sigma 18.82}$. Tarutinoite is monoclinic, space group *C*2/*m*, with *a* = 13.5447(12), *b* = 4.1027(3), *c* = 32.481(4) Å, β = 96.433(9)°, *V* = 1793.6(3) Å^3 and *Z* = 2. The strongest lines of the X-ray powder diffraction pattern [*d*, Å (*I*, %) (*hkl*)] are: 16.15 (48) (0 0 2), 3.407 (69) (1 1 -5), 3.328 (95) (2 0 -9), 3.042 (65) (2 0 -10), 2.941 (100) (3 1 2), 2.910 (55) (3 1 -4), 2.053 (44) (0 2 0). The crystal structure of tarutinoite was refined to R_1 = 0.1349 for 2024 reflections with $F_o > 4\sigma(F_o)$ and 84 refined parameters. The new mineral is the first $^{7,8}L$ member of the lillianite homologous series. It is named after its type locality.

Keywords: tarutinoite; new mineral; chemical composition; crystal structure; lillianite homologous series; Tarutinskoe deposit; Southern Urals; Russia

Introduction

The lillianite homologous series include numerous complex Ag-Pb-(Bi,Sb)-bearing sulfosalts and is derived from the structure of lillianite, $Pb_3Bi_2S_6$. Members of this series have structures consisting of alternating layers of PbS archetype cut parallel to $(311)_{PbS}$. The octahedra of adjacent, mirror-related layers are replaced by bicapped trigonal coordination prisms of PbS_{6+2} with the Pb atoms located on the mirror planes (e.g., Pažout, 2017). Detailed description of this series can be found in several publications (e.g., Makovicky and Karup-Møller, 1977a; Makovicky and Topa, 2014; Topa *et al.*, 2016; Pažout, 2017).

Existing members of the lillianite homologous series can be divided into the lillianite branch (Bi-dominant members) and the andorite branch (Sb-dominant members). They can be described as $^{N1,N2}L$ (*L* = lillianite homologue), where N1 and N2 are the numbers of octahedra for two adjacent sets of layers. They can be equal (known combinations for existing minerals are 4–4, 7–7, 8–8 or 11–11) or different (known combinations are 4–7, 4–8 and 5–9).

In the course of the study by scanning electron microscopy with energy-dispersive spectrometry (SEM-EDS) and ore microscopy of the old-collected samples of drill core from the Tarutinskoe (Tarutino) copper-skarn deposit, Southern Urals, Russia, we encountered an Ag-Pb-

Bi sulfosalt with a stoichiometry differing from all the already existing lillianite homologous series' members. Subsequent investigations of its crystal structure in combination with wavelength-dispersive spectroscopy (WDS) showed this phase to be a new $^{7,8}L$ member of the lillianite branch. It was named tarutinoite after its type locality. The new mineral, its name and symbol (Trtn) have been approved by the Commission on New Minerals, Nomenclature and Classification of the International Mineralogical Association (CNMNC-IMA) (IMA2023–122, Kasatkin *et al.*, 2024). The holotype specimen is deposited in the systematic collection of the Fersman Mineralogical Museum of the Russian Academy of Sciences, Moscow, with the catalogue number 98571.

Occurrence and general appearance

The new mineral occurs at the Tarutinskoe (Tarutino) copper-skarn deposit, 9.5 km S of the Tarutino village, 220 km S of Chelyabinsk, Chesmensk district, Chelyabinsk Oblast, Southern Urals, Russia (latitude 53° 70' 89" N, longitude 61° 02' 90" E) (Fig. 1).

The Tarutinskoe deposit is located at the southern contact of the Yuzhno-Karamysovsky massif of diorites and plagiogranites and volcano-sedimentary strata of Siluro-Devonian age (Fig. 2). Skarn zones formed after the remnants of marbles and host granitoids, and they consist of skarn bodies up to 100 m long and 28 m thick. The majority of magnetite-sulfidic and sulfide orebodies are confined to skarns while only few are located in the zones of moderately to strongly sericitized granitoids. Main gangue minerals of the skarns include garnets (andradite, grossular), epidote, chlorites (clinochlore, chamosite), pyroxenes (diopside, hedenbergite), amphiboles (actinolite, tremolite) and calcite. Main ore minerals comprise magnetite, hematite and sulfides (pyrite, chalcopyrite, galena, sphalerite). More detailed description of the Tarutinskoe deposit, its geology and mineralogy can be found elsewhere (Grabezhev *et al.*, 2002, 2004, 2005; Grabezhev and Shardakova, 2006; Grabezhev and Ronkin, 2007; *etc*.).

Tarutinoite was found in a fragment of a drill core extracted at 178.5 m level of borehole #4604 (Fig. 3) as anhedral grains up to 0.10 × 0.05 mm in magnetite-calcite matrix (Figs 4a, b). Apart the two latter, the drill core is composed of major pyrite, chalcopyrite and andradite. Other associated minerals include aikinite, baryte, berryite, bismuthinite, clinochlore, galena, hessite, quartz, scheelite and tetradymite.

Tarutinoite most probably crystallized from hydrothermal fluids during the ore-forming stage.

Physical properties and optical data

Tarutinoite is grey, opaque with metallic luster, brittle tenacity and uneven fracture. No cleavage and parting are observed. The Vickers' micro-indentation hardness (VHN, 25 g load) is 178 kg/mm^2 (range 165–194, n = 4), corresponding to a Mohs' hardness of 3.5–4. The density of the mineral could not be measured due to the very small amount of available material and absence of necessary heavy liquids. A density value calculated using the empirical formula and unit-cell volume obtained from single-crystal X-ray diffraction (SCXRD) data is 7.180 g/cm^3. In reflected light, tarutinoite is greyish-white, very slightly brighter than neighbouring galena, very weakly bireflectant and non-pleochroic. In crossed polarizers the new mineral exhibits moderate anisotropy, in grey and dark grey tones with bluish tints. Reflectance values have been measured in air using an MSF-R (LOMO, Saint-Petersburg, Russia) microspectrophotometer. Silicon was used as a standard. The reflectance values (R_{max}/R_{min}) are given in Table 1 and plotted in Fig. 5.

Chemical Data

Quantitative chemical analyses were carried out using a Cameca SX 100 electron microprobe (WDS mode, 25 kV, 4 nA, 3 μm beam diameter) at the Department of Geological Sciences, Faculty of Science, Masaryk University, Brno, Czech Republic. Observation in back-scattered electron (BSE) mode (Fig. 4b) and chemical microanalyses revealed homogeneous chemical composition of tarutinoite. Results (average of 7 spot analyses) and list of standards are given in Table 2. Contents of other elements with atomic numbers >8 (including Fe, As and Sb) are below detection limits. Matrix correction of X-PHI algorithm (Merlet, 1994) was applied to the data.

The empirical formula calculated on the basis of 36 atoms per formula unit is $(Ag_{3.01}Cu_{0.18})_{\Sigma 3.19}(Pb_{6.98}Cd_{0.01})_{\Sigma 6.99}Bi_{7.00}(S_{18.42}Se_{0.20}Te_{0.20})_{\Sigma 18.82}$. The electrostatic valence Ev(%), defined as $\{[Ev(+) - Ev(-)]\times 100/[Ev(-)]\}$, is +1.4%. The simplified formula of tarutinoite is $(Ag,Cu)_3(Pb,Cd)_7Bi_7(S,Se,Te)_{19}$.

The ideal formula of tarutinoite is $Ag_3Pb_7Bi_7S_{19}$, which requires (in wt.%) Ag 8.41, Pb 37.71, Bi 38.04, S 15.84, total 100.00

X-ray Crystallography

Powder X-ray diffraction (PXRD) data were collected by means of a Rigaku R-AXIS Rapid II single-crystal diffractometer equipped with a cylindrical image plate detector (radius 127.4 mm) using a Debye-Scherrer geometry, Co$K\alpha$ radiation (rotating anode with VariMAX microfocus optics), 40 kV and 15 mA. The angular resolution of the detector is 0.045° 2θ (pixel size 0.1 mm). The data were integrated using the software package *Osc2Tab* (Britvin et al.,

2017). PXRD data of tarutinoite are given in Table 4 in comparison to that calculated from SCXRD data using the *Vesta* program (Momma and Izumi, 2011). Parameters of monoclinic unit cell were refined from the observed *d* spacing data using *UnitCell* software (Holland and Redfern, 1997) and are as follows: a = 13.542(6), b = 4.107(3), c = 32.522(8) Å, β = 96.498(7)°, V = 1797.3(9) Å^3. It should be noted that due to the lack of material, PXRD data were collected from the same grain which was used for SCXRD studies (see below). This issue with the preferential orientation of the single crystal during PXRD data collection also introduces a difference in the intensity of the peaks in the observed and calculated powder diffraction patterns while maintaining their angular positions (Table 3).

For the SCXRD study, a grain of tarutinoite, 0.080 × 0.070 × 0.020 mm^3 in size, manually extracted from the polished section analysed using electron microprobe (Fig. 4b), was mounted on a glass fiber and examined through a Supernova Rigaku-Oxford Diffraction diffractometer equipped with a micro-source Mo*K*α radiation (λ = 0.71073 Å; 50 kV, 0.8 mA) and a Pilatus 200K Dectris detector at the Dipartimento di Geoscienze (University of Padua, Italy). We collected intensity data over 27 runs (for a total of 1719 frames) and an exposure time of 26 seconds per degree of omega rotation for a total time of 12.33 hours. The data were processed by *CrysAlisPro* 1.171.41.123a software (Rigaku Oxford Diffraction) and are as follows: tarutinoite is monoclinic, space group *C*2/*m*, with unit-cell parameters a = 13.5447(12), b = 4.1027(3), c = 32.481(4) Å, β = 96.433(9)°, V = 1793.6(3) Å^3 and Z = 2.

The crystal structure of tarutinoite was solved using *Shelxs*-97 in the space group *C*2/*m* and refined using *Shelxl*-2018 (Sheldrick, 2015). Neutral scattering curves for Ag, Pb, Bi, and S were taken from the *International Tables for Crystallography* (Wilson, 1992). Nine cation and ten anion sites were located. The initial structural model refined to R_1 = 0.195 and was improved to R_1 = 0.157 after modelling the occurrence of twinning according to a two-fold axis along [100]. The site occupancies at the *M*(1)–*M*(9) sites were modelled considering both site scattering and bond-valence sums (using the bond parameters of Brese and O'Keeffe, 1991). Indeed, Pb (Z = 82) and Bi (Z = 83) cannot be distinguished on the basis of site scattering only, and their site occupancies were fixed on the basis of the bond-valence approach. *M*(1) and *M*(5) sites were found to host Ag and a heavier element; on the basis of bond-valence sums, a mixed (Ag/Bi) occupancy was refined. Silver occurs also at the *M*(7) and *M*(8) positions. At the former, it occurs along with Pb, whereas at the latter site a mixed (Pb,Bi,Ag) occupancy was modelled, initally refining the Pb *vs*. Ag site occupancy and then adjusting the Pb/Bi ratio to optimize the bond-valence sum. *M*(6) and *M*(9) were modelled as pure Bi and Pb positions, whereas some mixed (Pb/Bi) sites were identified, namely *M*(2), *M*(3), and *M*(4). In particular, the *M*(3) site was found to be split into two sub-positions: the *M*(3a)/*M*(3b) site occupancy was initially

refined and then the Pb/Bi ratio at the two sub-sites was fixed on the basis of bond-valence sums. Whereas the displacement parameters of cation positions were refined anisotropically (with the exception of the split M(3) position), the parameters of anion sites were modelled using isotropic displacement parameters, as some of them were negatively defined using the anisotropic model. After several cycles of refinement, the R_1 converged to 0.1349 on the basis of 2024 unique reflections with $Fo > 4\sigma(Fo)$ and 84 refined parameters.

Details of data collection and refinement are given in Table 4. Fractional atomic coordinates, site occupancies, and displacement parameters are reported in Table 5. Table 6 reports selected bond distances. Table 7 gives the weighted bond-valence calculations calculated using the bond-valence parameters of Brese and O'Keeffe (1991). Supplementary crystallographic data were deposited in the Inorganic Crystal Structure Database (ICSD) and can be obtained by quoting the CSD 2380182 *via* www.ccdc.cam.ac.uk/structures/, and is available as Supplementary material (see below).

Crystal structure description

The features of the crystal structure of tarutinoite (Fig. 6) agree with those of the members of the lillianite homologous series (e.g., Makovicky and Karup-Møller, 1977a; Makovicky and Topa, 2014). Tarutinoite shows two different kinds of PbS-like slabs, parallel to (001). Lead atoms on the composition planes of the unit-cell twinning (according to the definition first given by Andersson and Hyde, 1974) show a bicapped trigonal prismatic coordination.

The two different slabs have a different diagonal width of the PbS-like octahedral layers, i.e., seven and eight, respectively.

The thinner (N = 7) t slab has composition $^{M(1)}(Ag_{0.92}Bi_{1.08})^{M(2)}(Bi_{1.60}Pb_{0.40})^{M(3)}(Pb_{1.78}Bi_{0.22})^{M(4)}(Pb_{0.50}Bi_{0.50})S_8 = Ag_{0.9}Pb_{2.68}Bi_{3.42}S_8$ (Z = 2). The M(1) site is a mixed (Bi,Ag) site, with site occupancy $Ag_{0.46(5)}Bi_{0.54(5)}$. It shows three distances distinctly shorter than 3 Å (average <Ag–S> distance of 2.67 Å), and three longer ones, ranging between 2.98 and 3.07 Å. Bond-valence sum (BVS) at the M(1) site is 2.10 valence units (v.u.), agreeing with theoretical value based on site occupancy. The M(2) site is a mixed (Bi,Pb) site, with a Bi/(Bi+Pb) ratio of 0.8. The average <M(2)–S> is 2.87 Å. The octahedral coordination of this position is characterized by five Bi–S distances shorter than 3 Å (average value of 2.82 Å) and a sixth long distance of 3.16 Å. The BVS value is 2.73 v.u. Electron density at the M(3) site was found to be split into two sub-positions, namely M(3a) and M(3b). This site was refined as a mixed (Pb,Bi) position. The sum of the BVSs at these two sub-sites is 2.10 v.u., to be compared with the calculated value of 2.12 v.u. on the basis of the site occupancy ($Pb_{0.89}Bi_{0.11}$). Finally, the M(4) site shows a nearly regular octahedral coordination, with average <M(4)–S> bond distance of

2.90 Å. The site occupancy was fixed to ($Pb_{0.50}Bi_{0.50}$) on the basis of the value of the BVS, i.e., 2.36 v.u. Sulfur sites belonging to this slab are S(1)-S(4). Their BVSs range between 1.82 and 2.10 v.u.

The thicker (N = 8) T slab has composition $^{M(5)}(Ag_{0.98}Bi_{1.02})_{\Sigma 2.00}\ ^{M(6)}Bi_2\ ^{M(7)}(Pb_{1.42}Ag_{0.58})_{\Sigma 2.00}\ ^{M(8)}(Pb_{1.00}Bi_{0.70}Ag_{0.30})_{\Sigma 2.00}S_9 = Ag_{1.86}Pb_{2.42}Bi_{3.72}S_9$ (Z = 2). The M(5) site shows a distorted octahedral coordination, with a mixed (Ag,Bi) occupancy, with three <M(5)–S> distances shorter than 3 Å (average 2.69 Å) and three longer ones (average 2.99 Å). The BVS, 2.13 v.u., agrees with the refined ($Ag_{0.49(4)}Bi_{0.51(4)}$) occupancy of this position. The M(6) site is a pure Bi position, with five distances shorter than 3 Å (average value of 2.79 Å) and the sixth ligand at 3.12 Å. Its BVS, 2.96 v.u., fully agrees with the occupancy by Bi^{3+}. The M(7) site is a mixed (Pb,Ag) position, with an average <M(7)–S> bond distance of 2.94 Å. The BVS value, 1.70 v.u., is in accordance with that calculated on the basis of the refined site occupancy $Pb_{0.71(5)}Ag_{0.29(5)}$. Finally, the M(8) site is a nearly regular octahedron with a mixed (Pb,Bi,Ag) occupany. The BVS, 2.12 v.u., can be compared with the theoretical one, i.e., 2.20 v.u. Anions, in this slab, are hosted at sites S(5)-S(9). Their BVS varies between 1.72 and 1.96 v.u.

The composition plane of the unit-cell twinning of tarutinoite is composed by the sites M(9) and S(10). The M(9) site is a pure Pb site, with a trigonal bicapped prismatic coordination, with an average bond distance of 3.14 Å. The BVS at this site is 1.84 v.u., whereas at the S(10) position is 2.42 v.u. The chemistry of this composition plane is $^{M(9)}Pb_2S_2$.

On the basis of the structural investigation, the formula of tarutinoite can be written as $^{t}[Ag_{0.92}Pb_{2.68}Bi_{3.40}S_8] + {}^{T}[Ag_{1.86}Pb_{2.42}Bi_{3.72}S_9] + Pb_2S_2 = Ag_{2.78}Pb_{7.10}Bi_{7.12}S_{19}$ (Z = 2), Ev = +0.9%. This formula agrees with the ideal one, $Ag_3Pb_7Bi_7S_{19}$ (Z = 2).

Notwithstanding the relatively high R value, i.e., 0.1349, the crystal structure of tarutinoite is physically sound, as proved by bond distances, bond-valence sums, and the fit between crystal structure and chemical composition. The high R value, as well as the relatively high residuals, could be due to the widespread twinning of tarutinoite [twin according to a two-fold axis along **a**, with a refined ratio between the two domains of 0.321(9)] and the possible occurrence of stacking disorder along the **c** direction.

Discussion

As shown above, tarutinoite is the first $^{7,8}L$ member of the lillianite homologous series. While the natural member was unknown up-to-now, such kind of a homologue was reported in synthetic runs using high resolution transmission electron microscopy by Skowron and Tilley (1990). Tarutinoite is the 13th member of the lillianite branch within the lillianite homologous series. Their comparison is given in Table 8.

The empirical formula of tarutinoite can be written as $Cu_{0.18}Ag_{3.01}Cd_{0.01}Pb_{6.98}Bi_{7.00}S_{18.42}Se_{0.20}Te_{0.20}$. Considering homovalent substitutions $Cd^{2+} = Pb^{2+}$, $Se^{2-} = S^{2-}$, and $Te^{2-} = S^{2-}$, this formula can be modified to $Cu_{0.18}Ag_{3.01}Pb_{6.99}Bi_{7.00}S_{18.82}$. Copper is probably hosted in tetrahedral voids within the crystal structure of tarutinoite, as observed in other lead sulfosalts (e.g., bournonite, Edenharter *et al*., 1970; zinkenite, Biagioni *et al*., 2018). Unfortunately, owing to its relatively low abundance and the low quality of the structure refinement, this hypothesis cannot be experimentally confirmed. However, following Makovicky and Karup-Møller (1977a), Cu was excluded from the calculation of the homologue order. The homologue order of tarutinoite, calculated in agreement with Makovicky (2019) and references therein, is N_{chem} = 7.52; the mole fraction of the Ag–Bi end-member L = 54.65%, and the substitution parameter in the general formula $Ag_xPb_{N-1-2x}Bi_{2+x}S_{N+2}$ is x = 1.51. Ideal tarutinoite, $Ag_3Pb_7Bi_7S_{19}$ has N_{chem} = 7.50, L = 54.55% and x = 1.50, in agreement with values calculated from the empirical formula. This probably suggests the correctness of the assumption about the Cu role in tarutinoite.

Supplementary material

To view supplementary material for this article, please visit: https://doi.org/...

Acknowledgements

We thank Associate Editor Owen Missen and two anonymous Reviewers for constructive comments that improved the manuscript. Maria D. Milshina is acknowledged for the help with the figures. The PXRD studies have been performed at the Research Centre for X-ray Diffraction Studies of St. Petersburg State University within the framework of the project AAAA-A19-119091190094-6.

References

Andersson S. and Hyde B.G. (1974) Twinning on the unit cell level as a structure-building operation in the solid state. *Journal of Solid State Chemistry*, **9**, 92–101.

Berlepsch P., Armbruster T., Makovicky E., Hejny C., Topa D. and Graeser S. (2001) The crystal structure of (001) twinned xilingolite, $Pb_3Bi_2S_6$, from Mittal-Hohten, Valais, Switzerland. *The Canadian Mineralogist*, **39**, 1653–1663.

Biagioni C., Bindi L. and Moëlo Y. (2018) Another step toward the solution of the real structure of zinkenite. *Zeitschrift für Kristallographie – Crystalline Materials*, **233**, 269–277.

Brese N.E. and O'Keeffe M. (1991) Bond-valence parameters for solids. *Acta Crystallographica*, **B47**, 192–197.

Britvin S.N., Dolivo-Dobrovolsky D.V. and Krzhizhanovskaya M.G. (2017) Software for processing the X-ray powder diffraction data obtained from the curved image plate detector of Rigaku RAXIS Rapid II diffractometer. *Zapiski Rossiiskogo Mineralogicheskogo Obshchestva*, **146**, 104–107 (in Russian).

Callegari A.M. and Boiocchi M. (2009) Aschamalmite ($Pb_6Bi_2S_9$): crystal structure and ordering scheme for Pb and Bi atoms. *Mineralogical Magazine*, **73**, 83–94.

Edenharter A., Nowacki W. and Takéuchi Y. (1970) Verfeinerung der kristallstruktur von bournonit [$(SbS_3)_2|Cu^{IV}{}_2Pb^{VII}Pb^{VIII}$] und von seligmannit [$(AsS_3)_2|$ $Cu^{IV}{}_2Pb^{VII}Pb^{VIII}$]. *Zeitschrift für Kristallographie*, **131**, 397–417 (in German).

Grabezhev A.I. and Ronkin Yu.L. (2007) Carbon, oxygen and strontium isotopes in copper-skarn deposits of the Urals. *Litosphere*, **4**, 102–114 (in Russian).

Grabezhev A.I. and Shardakova G.Yu. (2006) Ore-bearing granitoids of Uralian copper-skarn deposits: petrogeochemistry in connection with ore-metasomatic zonality features. *Litosphere*, **4**, 68–78 (in Russian).

Grabezhev A.I., Belgorodsky E.A., Sotnikov V.I. and Gmyrya V.G. (2002) Skarns of Tarutino skarn-porphyry copper deposit, Southern Urals. *Petrology*, **10**(1), 46–59 (in Russian).

Grabezhev A.I., Gmyra V.G., Vigorova V.G. and Palgueva G.V. (2005) Garnets from skarns of Gumeshevskoe and Tarutinskoe skarn-copper-porphyry deposits. *Bulletin of the Ural Branch of the Russian Academy of Sciences*, **4**, 55–60 (in Russian).

Grabezhev A.I., Sotnikov V.I., Belgorodsky E.A., Murzin V.V. and Moloshag V.P. (2004) Acid leaching in skarn-copper-porphyry systems: Tarutino deposit, Southern Urals. *Geology of ore deposits*, **46**(6), 510–523 (in Russian).

Holland T.J.B. and Redfern S.A.T. (1997) Unit cell refinement from powder diffraction data: the use of regression diagnostics. *Mineralogical Magazine*, **61**, 65–77.

Kasatkin A.V., Biagioni C., Nestola F., Škoda R., Gurzhiy V.V., Agakhanov A.A. and Kuznetsov A.M. (2024) Tarutinoite, IMA 2023–122, in: CNMNC Newsletter 79, *European Journal of Mineralogy*, **36**, 525–528.

Makovicky E. (2019) Algorithms for calculation of homologue order *N* in the homologous series of sulfosalts. *European Journal of Mineralogy*, **31**, 83–97.

Makovicky E. and Karup-Møller S. (1977a) Chemistry and crystallography of the lillianite homologous series. Part I: General properties and definitions. *Neues Jahrbuch für Mineralogie, Abhandlungen*, **130**, 264–287.

Makovicky E. and Karup-Møller S. (1977b) Chemistry and crystallography of the lillianite homologous series. Part II: Definition of new minerals: eskimoite, vikingite, ourayite and treasurite. Redefinition of schirmerite and new data on the lillianite-gustavite solid solution series. *Neues Jahrbuch für Mineralogie, Abhandlungen*, **131**, 56– 82.

Makovicky E. and Topa D. (2011) The crystal structure of gustavite, $PbAgBi_3S_6$. Analysis of twinning and polytypism using the OD approach. *European Journal of Mineralogy*, **23**, 537–550.

Makovicky E. and Topa D. (2014) Lillianites and andorites: new life for the oldest homologous series of sulfosalts. *Mineralogical Magazine*, **78**, 387–414.

Makovicky E., Mumme W.G. and Madsen I.C. (1992) The crystal structure of vikingite. *Neues Jahrbuch für Mineralogie, Monatshefte*, **1992/10**, 454–468.

Merlet C. (1994) An Accurate Computer Correction Program for Quantitative Electron Probe Microanalysis. *Microchimica Acta*, **114/115**, 363–376.

Momma K. and Izumi F. (2011) VESTA 3 for three-dimensional visualization of crystal, volumetric and morphology data. *Journal of Applied Crystallography*, **44**, 1272–1276.

Pažout R. (2017) Lillianite homologues from Kutná Hora ore district, Czech Republic: a case of large-scale Sb for Bi substitution. *Journal of Geosciences*, **62**, 37–57.

Pažout R. and Sejkora J. (2018) Staročeskéite, $Ag_{0.70}Pb_{1.60}(Bi_{1.35}Sb_{1.35})_{\Sigma 2.70}S_6$, from Kutná Hora, Czech Republic, a new member of the lillianite homologous series. *Mineralogical Magazine*, **82**, 993–1005.

Pinto D., Balić-Žunić T., Garavelli A., Makovicky E. and Vurro F. (2006) Comparative crystal-structure study of Ag-free lillianite and galenobismutite from Vulcano, Aeolian Islands, Italy. *The Canadian Mineralogist*, **44**, 159–175.

Pinto D., Balić-Žunić T., Garavelli A. and Vurro F. (2011) Structure refinement of Ag-free heyrovskýite from Vulcano (Aeolian Islands, Italy). *American Mineralogist*, **96**, 1120–1128.

Sheldrick G.M. (2015) Crystal structure refinement with SHELXL. *Acta Crystallographica*, **C71**, 3–8.

Skowron A. and Tilley J.D. (1990) Chemically twinned phases in the Ag_2S–PbS–Bi_2S_3 system. Part I. Electron microscope study. *Journal of Solid State Chemistry*, **85**, 235–250.

Topa D., Makovicky E., Zagler G., Putz H. and Paar W.H. (2013) Erzwiesite, IMA 2012-082. CNMNC Newsletter No. 15, February 2013, page 11. *Mineralogical Magazine*, **77**, 1–12.

Topa D., Makovicky E., Stanley C.J. and Roberts A.C. (2016) Oscarkempffite, $Ag_{10}Pb_4(Sb_{17}Bi_9)_{\Sigma=26}S_{48}$, a new Sb-Bi member of the lillianite homologous series, *Mineralogical Magazine*, **80**, 809–817.

Yang H., Downs R.T., Evans S.H. and Pinch W.W. (2013) Terrywallaceite, $AgPb(Sb,Bi)_3S_6$, isotypic with gustavite, a new mineral from Mina Herminia, Julcani Mining District, Huancavelica, Peru. *American Mineralogist*, **98**, 1310–1314.

Wilson A.J.C. (editor) (1992) *International Tables for Crystallography Volume C: Mathematical, Physical and Chemical Tables*. Kluwer Academic Publishers, Dordrecht, The Netherlands.

Table 1. Reflectance values for tarutinoite (COM standard wavelengths are given in bold).

λ (nm)	R_{max}	R_{min}		λ (nm)	R_{max}	R_{min}
400	54.7	52.0		560	44.6	43.4
420	52.4	50.0		580	44.2	43.3
440	49.9	47.2		**589**	**44.1**	**43.3**
460	48.4	45.9		600	44.0	43.2
470	**47.9**	**45.5**		620	43.4	42.7
480	47.3	45.1		640	43.0	42.2
500	46.5	44.4		**650**	**42.5**	**41.8**
520	45.8	44.3		660	42.0	41.3
540	45.2	43.5		680	39.9	39.2
546	**45.0**	**43.5**		700	37.8	37.1

Table 2. Chemical data (in wt. %) for tarutinoite.

Element	Mean	Range (n = 7)	S.D.	Standard
Cu	0.30	0.27 – 0.35	0.03	Cu
Ag	8.33	8.14 – 8.65	0.20	Ag
Cd	0.04	0.00 – 0.13	0.05	Cd
Pb	37.12	36.27 – 38.02	0.65	PbSe
Bi	37.52	36.61 – 38.48	0.73	Bi
S	15.15	14.78 – 15.76	0.33	chalcopyrite
Se	0.40	0.31 – 0.48	0.08	PbSe
Te	0.66	0.61 – 0.77	0.05	HgTe
Total	99.52			

S.D. = standard deviation; n = number of spot analyses.

Table 3. Powder X-ray diffraction data (*d* in Å) of tarutinoite.

d_{obs}		I_{obs}	d_{calc}*	I_{calc}**	*h k l*	d_{obs}	I_{obs}	d_{calc}*	I_{calc}**	*h k l*
16.15		**48**	16.14	16	0 0 2	**2.053**	**44**	2.051	62	0 2 0
			3.645	29	2 0 -8			2.049	15	6 0 5
3.622		8	3.619	43	2 0 7			2.049	29	5 1 -8
3.572		9	3.575	32	1 1 -4			2.017	17	1 1 -14
3.489		9	3.485	60	1 1 4			2.010	23	5 1 6
3.407		**69**	3.403	64	1 1 -5			2.006	7	6 0 -9
			3.386	9	4 0 -1	1.996	11	1.992	14	5 1 -9
			3.370	24	4 0 -2			1.905	5	3 1 -14
			3.365	29	4 0 0	1.904	7	1.899	17	0 0 17
3.328		**95**	3.323	84	2 0 -9			1.892	5	5 1 8
			3.319	21	4 0 -3			1.852	10	3 1 13
			3.309	21	4 0 1			1.831	6	5 1 9
3.304		10	3.306	54	1 1 5			1.820	9	3 1 -15
			3.301	58	2 0 8	1.816	10	1.811	6	5 1 -12
			3.237	7	4 0 -4			1.810	5	4 0 14
			3.221	21	1 1 -6	1.788	32	1.788	6	2 2 -8
3.042		**65**	3.046	23	2 0 -10			1.785	11	2 2 7
			3.036	12	3 1 -1			1.771	10	3 1 14
			3.027	35	2 0 9			1.770	5	5 1 10
			2.993	29	3 1 1			1.752	8	4 2 -2
			2.974	41	3 1 -3			1.752	8	4 2 0
2.941		**100**	2.934	75	3 1 2			1.751	8	5 1 -13
2.910		**55**	2.908	100	3 1 -4			1.750	5	7 1 -2
2.857		27	2.859	63	3 1 3			1.748	10	7 1 -1
2.824		9	2.824	39	3 1 -5			1.747	7	7 1 -3
			2.807	19	2 0 -11	1.749	16	1.746	25	2 2 -9
2.795		8	2.791	23	2 0 10			1.745	6	4 2 -3
2.764		5	2.767	5	3 1 4			1.743	7	4 2 1
2.248		5	2.253	7	1 1 -12			1.742	17	2 2 8
			2.186	29	1 1 12			1.739	9	4 0 -17
2.130		7	2.130	40	1 1 -13			1.727	8	4 0 15
			2.117	7	5 1 4	1.707	17	1.702	7	2 2 -10
			2.112	5	6 0 -7	1.700	5	1.698	10	2 2 9
			2.102	15	5 1 -7	1.672	6	1.674	6	8 0 -5
2.097		15	2.101	11	6 0 4			1.670	8	8 0 1
			2.068	22	1 1 13			1.662	5	4 0 -18
			2.066	31	5 1 5	1.658	5	1.660	6	8 0 -6
			2.061	20	6 0 -8			1.656	5	2 2 -11

* For the calculated pattern, only reflections with intensities ≥5 are given.
** For the unit-cell parameters calculated from single crystal data.
Strongest reflections are given in boldtype.

Table 4. Crystal and experimental data for tarutinoite.

Crystal data	
Crystal size (mm)	0.080 × 0.070 × 0.020
Space group	*C*2/*m*
a (Å)	13.5447(12)
b (Å)	4.1027(3)
c (Å)	32.481(4)
β (°)	96.433(9)
V (Å^3)	1793.6(3)
Z	2
Data collection and refinement	
Radiation, wavelength (Å)	Mo*K*α, λ = 0.71073
Temperature (K)	293(2)
$2\theta_{max}$ (°)	55.00
Measured reflections	15230
Unique reflections	2350
Reflections with $F_o > 4\sigma(F_o)$	2024
R_{int}	0.1273
$R\sigma$	0.0646
Range of *h*, *k*, *l*	$-17 \le h \le 17$, $-5 \le k \le 5$, $-42 \le l \le 42$
R_1 [$F_o > 4\sigma(F_o)$]	0.1349
R_1 (all data)	0.1440
wR_2 (on F_o^2)	0.3549
Goof	1.089
Number of least-squares parameters	84
Maximum and minimum residual peak (*e* Å^{-3})	+13.16 [at 0.77 Å from *M*(3a)] -10.80 [at 1.17 Å from S(5)]
ICSD	2380182

Table 5. Site, Wyckoff position, site occupancy, fractional atom coordinates, and equivalent isotropic or isotropic (*) displacement parameters ($Å^2$) in tarutinoite.

Site	Wyckoff Position	Site occupancy	*x*/*a*	*y*/*b*	*z*/*c*	$U_{eq/iso}$
M(1)	4*i*	$Ag_{0.46(5)}Bi_{0.54(5)}$	0.3725(5)	½	0.1682(2)	0.040(3)
M(2)	4*i*	$Bi_{0.80}Pb_{0.20}$	0.0777(3)	½	0.11465(13)	0.0196(9)
M(3a)	4*i*	$Pb_{0.675}Bi_{0.075}$	0.2125(3)	½	-0.05417(14)	0.0067(9)*
M(3b)	4*i*	$Pb_{0.2125}Bi_{0.0375}$	0.2087(10)	½	-0.0692(5)	0.0067(9)*
M(4)	2*a*	$Pb_{0.50}Bi_{0.50}$	0	0	0	0.0193(12)
M(5)	4*i*	$Ag_{0.49(4)}Bi_{0.51(4)}$	-0.0927(4)	0	0.30580(14)	0.0129(16)
M(6)	4*i*	$Bi_{1.00}$	0.1432(3)	½	0.35948(10)	0.0094(8)
M(7)	4*i*	$Pb_{0.71(5)}Ag_{0.29(5)}$	0.3855(3)	0	0.41691(14)	0.0189(16)
M(8)	4*i*	$Pb_{0.50}Bi_{0.35}Ag_{0.15}$	0.1291(3)	0	0.47260(12)	0.0208(10)
M(9)	4*i*	$Pb_{1.00}$	0.1577(4)	0	0.2374(2)	0.0335(11)
S(1)	4*i*	$S_{1.00}$	0.0026(19)	½	0.1866(8)	0.017(5)*
S(2)	4*i*	$S_{1.00}$	0.2089(18)	0	0.1422(7)	0.017(5)*
S(3)	4*i*	$S_{1.00}$	0.436(2)	½	0.0832(8)	0.022(6)*
S(4)	4*i*	$S_{1.00}$	0.1445(16)	½	0.0244(6)	0.009(4)*
S(5)	4*i*	$S_{1.00}$	0.037(2)	½	0.2886(8)	0.020(5)*
S(6)	4*i*	$S_{1.00}$	0.268(2)	0	0.3336(8)	0.022(5)*
S(7)	4*i*	$S_{1.00}$	0.524(2)	½	0.3898(8)	0.020(5)*
S(8)	4*i*	$S_{1.00}$	0.237(2)	0	0.5527(8)	0.031(7)*
S(9)	2*d*	$S_{1.00}$	0	½	½	0.020(7)*
S(10)	4*i*	$S_{1.00}$	0.3023(19)	½	0.2382(10)	0.025(5)*

Table 6. Selected bond distances (in Å) for tarutinoite.

M(1)	–S(10)	2.56(3)	*M*(2)	–S(1)	2.65(3)	*M*(3a)	–S(4)	2.81(2)
	–S(1)	2.727(17) ×2		–S(2)	2.794(17) ×2		–S(4)	2.910(15) ×2
	–S(3)	2.98(3)		–S(3)	2.92(2) ×2		–S(3)	2.95(2) ×2
	–S(2)	3.068(19) ×2		–S(4)	3.16(2)		–S(2)	3.16(2)
	average	2.86		average	2.87		average	2.95
M(3b)	–S(2)	2.73(3)	*M*(4)	–S(4)	2.885(14) ×4	*M*(5)	–S(10)	2.48(3)
	–S(3)	2.84(2) ×2		–S(3)	2.93(3) ×2		–S(5)	2.801(18) ×2
	–S(4)	3.103(18) ×2		average	2.90		–S(6)	2.99(2) ×2
	–S(4)	3.25(2)					–S(7)	2.99(3)
	average	2.98					average	2.84
M(6)	–S(5)	2.57(3)	*M*(7)	–S(8)	2.88(2) ×2	*M*(8)	–S(8)	2.84(3)
	–S(6)	2.85(2) ×2		–S(9)	2.958(4)		–S(9)	2.900(3) ×2
	–S(7)	2.856(19) ×2		–S(7)	2.98(2) ×2		–S(7)	2.90(3)
	–S(8)	3.12(3)		–S(6)	2.98(3)		–S(8)	2.92(2) ×2
	average	2.85		average	2.94		average	2.90
M(9)	–S(10)	2.834(18) ×2						
	–S(5)	3.20(2) ×2						
	–S(2)	3.25(3)						
	–S(1)	3.25(2) ×2						
	–S(6)	3.31(3)						
	average	3.14						

Table 7. Weighted bond valence (in valence unit) for tarutinoite.

Site	S(1)	S(2)	S(3)	S(4)	S(5)	S(6)	S(7)	S(8)	S(9)	S(10)	Σcations	Theor.
M(1)	$^{2\times\rightarrow}0.43^{\downarrow 2\times}$	$^{2\times\rightarrow}0.17^{\downarrow 2\times}$	0.22							0.68	2.10	2.08
M(2)	0.76	$^{2\times\rightarrow}0.52^{\downarrow 2\times}$	$^{2\times\rightarrow}0.37^{\downarrow 2\times}$	0.19							2.73	2.60
M(3a)		0.14	$^{2\times\rightarrow}0.25^{\downarrow 2\times}$	0.37 $^{2\times\rightarrow}0.28^{\downarrow 2\times}$							1.57	1.58
M(3b)		0.15	0.11 0.11	$^{2\times\rightarrow}0.06^{\downarrow 2}$ 0.04							0.53	0.54
M(4)			$^{2\times\rightarrow}0.36$	$^{4\times\rightarrow}0.41^{\downarrow 2\times}$							2.36	2.50
M(5)					$^{2\times\rightarrow}0.34^{\downarrow 2\times}$	$^{2\times\rightarrow}0.21^{\downarrow 2\times}$	0.21			0.82	2.13	2.02
M(6)					0.95	$^{2\times\rightarrow}0.46^{\downarrow 2\times}$	$^{2\times\rightarrow}0.44^{\downarrow 2\times}$	0.21			2.96	3.00
M(7)						0.25	$^{2\times\rightarrow}0.26^{\downarrow 2\times}$	$^{2\times\rightarrow}0.33^{\downarrow 2\times}$	$0.27^{\downarrow 2\times}$		1.70	1.71
M(8)							0.35	$^{2\times\rightarrow}0.33^{\downarrow 2\times}$ 0.41	$^{2\times\rightarrow}0.35^{\downarrow 4\times}$		2.12	2.20
M(9)	$^{2\times\rightarrow}0.15^{\downarrow 2\times}$	0.15			$^{2\times\rightarrow}0.17^{\downarrow 2}$	0.13				$^{2\times\rightarrow}0.46^{\downarrow 2\times}$	1.84	2.00
Σanions	1.92	1.82	2.04	2.10	1.97	1.72	1.96	1.94	1.94	2.42		
Theor.	2.00	2.00	2.00	2.00	2.00	2.00	2.00	2.00	2.00	2.00		

Table 8. Members of the lillianite branch within the lillianite homologous series.

Mineral	**Chemical formula**	***mol%*** $^{N}_{AgBiL}$	***a*** **(Å)**	***b*** **(Å)**	***c*** **(Å)**	**β (°)**	**s.g.**	**Ref.**
N = 4,4								
Lillianite	$Pb_3Bi_2S_6$	0.0%	13.57	20.66	4.12		*Bbmm*	[1]
Xilingolite	$Pb_3Bi_2S_6$	0.0%	13.51	4.08	20.65	92.2	*C*2/*m*	[2]
Gustavite	$AgPbBi_3S_6$	100.0%	7.06	19.69	8.22	107.0	$P2_1/c$	[3]
Staročeskéite	$Ag_{0.70}Pb_{1.60}(Bi_{1.35}Sb_{1.35})S_6$	70.0%	4.25	13.31	19.62		*Cmcm*	[4]
Terrywallaceite	$AgPb(Bi,Sb)_2(Sb,Bi)S_6$	100%	6.98	19.35	8.39	107.5	$P2_1/c$	[5]
N = 4,7								
Vikingite	$Ag_5Pb_8Bi_{13}S_{30}$	71.4%	13.60	4.11	25.25	95.6	*C*2/*m*	[6]
N = 4,8								
Treasurite	$Ag_7Pb_6Bi_{15}S_{32}$	87.5%	13.35	26.54	4.09	92.8	*B*2/*m*, *B*2 or *Bm*	[7]
N = 5,9								
Eskimoite	$Ag_7Pb_{10}Bi_{15}S_{36}$	70.0%	13.46	30.19	4.10	93.4	*B*2/*m* or *Bm*	[7]
N = 7,7								
Aschamalmite	$Pb_6Bi_2S_9$	0.0%	13.72	4.13	31.42	90.9	*C*2/*m*	[8]
Heyrovskýite	$Pb_6Bi_2S_9$	0.0%	13.75	31.51	4.15		*Bbmm*	[9]
N = 7,8								
Tarutinoite	$Ag_3Pb_7Bi_7S_{19}$	54.6%	13.55	4.10	32.48	96.4	*C*2/*m*	[10]
N = 8,8								

Erzwiesite	$Ag_8Pb_{12}Bi_{16}S_{40}$	66.7%	4.08	13.46	33.92		*Cmcm*	[11]
N = 11,11 Ourayite	$Ag_3Pb_4Bi_5S_{13}$	66.7%	13.45	44.04	4.10		*Bbmm* or $Bb2_1m$	[7]

N = homologue order. [1] Pinto *et al*. (2006); [2] Berlepsch *et al*. (2001); [3] Makovicky and Topa (2011); [4] Pažout and Sejkora (2018); [5] Yang *et al*. (2013); [6] Makovicky *et al*. (1992); [7] Makovicky and Karup-Møller (1977b); [8] Callegari and Boiocchi (2009); [9] Pinto *et al*. (2011); [10] this paper; [11] Topa *et al*. (2013).

Figure 1. The Tarutinskoe copper-skarn deposit. The soil parts are results of prospecting workings. June 2015. Photo by Aleksey Podkorytov.

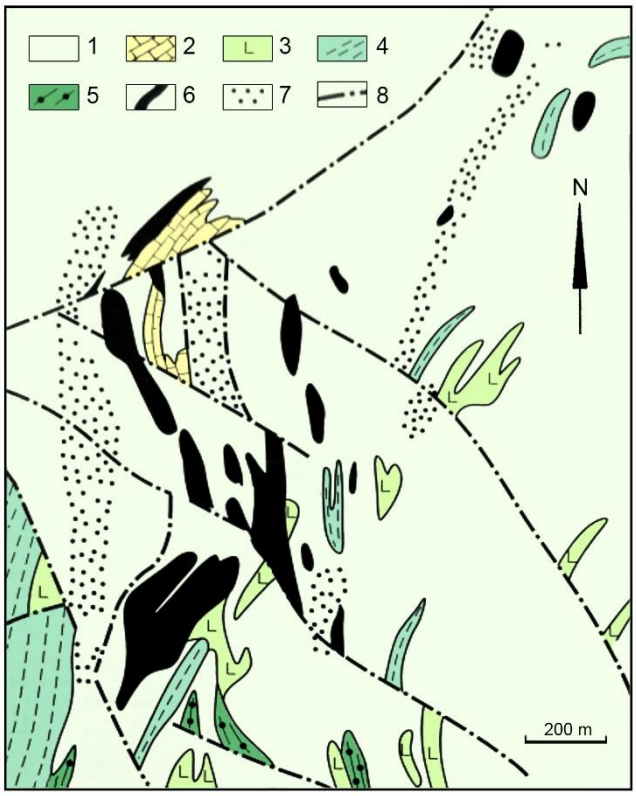

Figure 2. Geologic map of the Tarutinskoe deposit (modified after Grabezhev *et al.*, 2004): 1 – Quartz diorites and plagiogranodiorites, 2 – metalimestones, 3 – basalt aphyrites, 4 – tuff aleurolites, sandstones, 5 – tuff sandstones and arkosic sandstones, 6 – skarns and aposkarn orebodies, 7 – zones of moderate and strong sericitization of granitoids with veinlet-disseminated mineralization, 8 – tectonic faults.

Figure 3. Fragment of drill core where tarutinoite was found. Dark areas are mainly composed of magnetite, chalcopyrite, pyrite and andradite. White is calcite. Size: 8 × 4 × 2 cm. Photo by Aleksey Podkorytov.

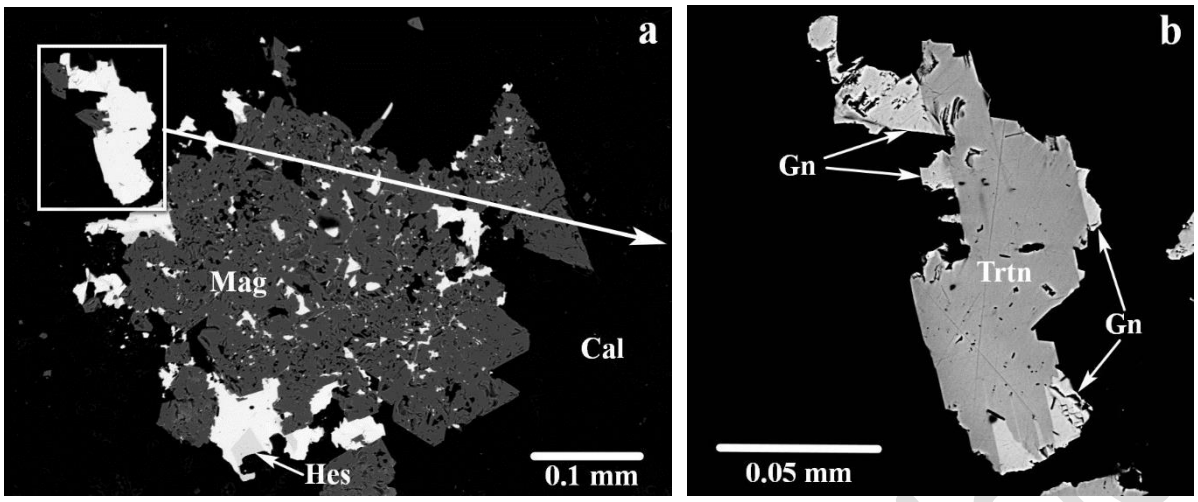

Figure 4: a) Tarutinoite (white grains) with hessite (Hes) in magnetite (Mag) and calcite (Cal); **b)** magnified fragment of Fig. 3a, with different degrees of contrast and brightness applied in order to make possible the identification of the different phases: tarutinoite (Trtn) grain intergrown with galena (Gn). Part of this grain was extracted for SCXRD studies. Polished section. SEM (BSE) image.

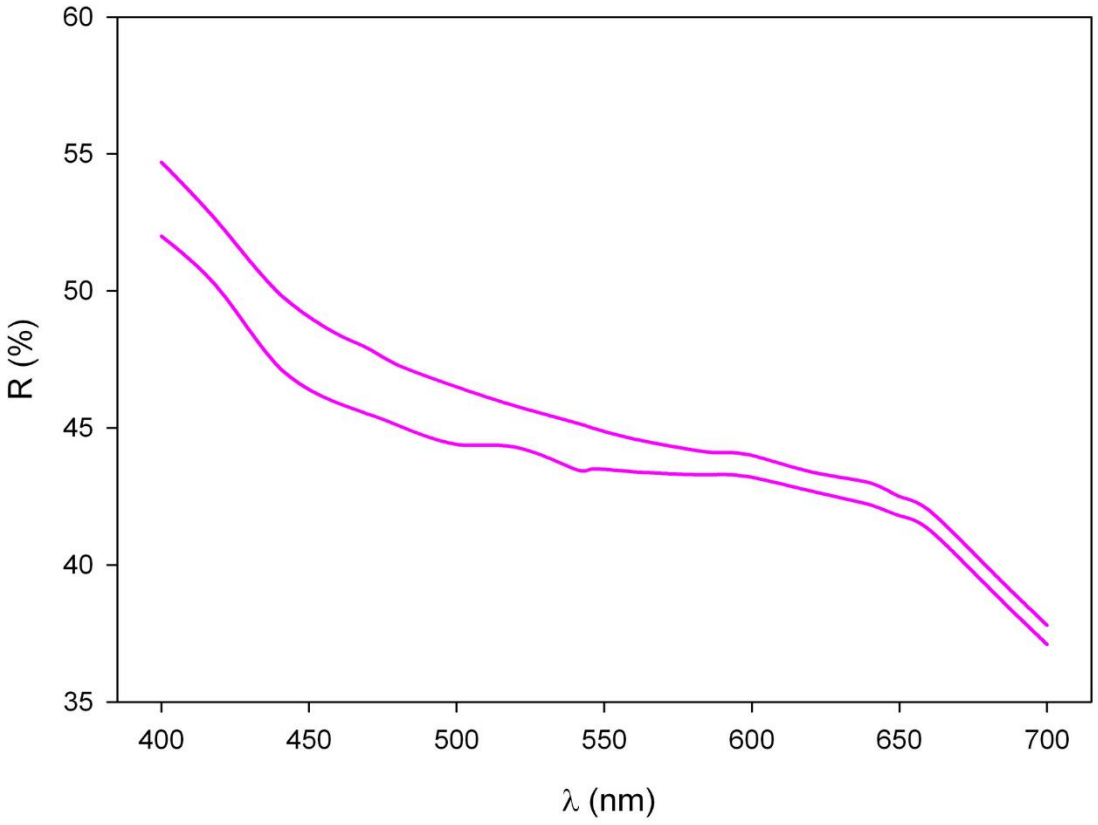

Figure 5. Reflectance curves of tarutinoite.

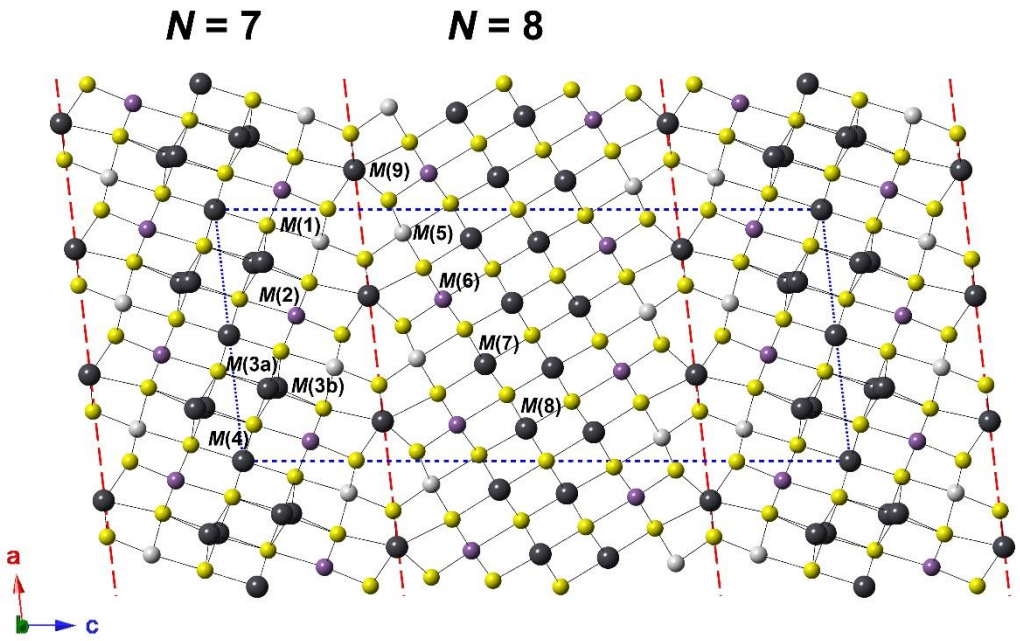

Figure 6. Crystal structure of tarutinoite as seen down **b**. Violet, grey, dark grey and yellow circles represent Bi-dominant, mixed (Ag/Bi), Pb-dominant, and S-hosting sites. Red lines indicate the composition planes of the unit-cell twinning separating the $N = 7$ and $N = 8$ slabs.